SCATSAT-1 Scatterometer: an improved successor of OSCAT

T. Misra, P. Chakraborty*, C. Lad, P. Gupta, J. Rao, G. Upadhyay, S. Vinay Kumar, B. Saravana Kumar, S. Gangele, S. Sinha, H. Tolani, V. K. Vithani, B. S. Raman, C. V. N. Rao, D. B. Dave, R. Jyoti and N. M. Desai

Space Applications Centre, ISRO, Ahmedabad 380 015, India

SCATSAT-1 is the Indian Space Research Organisation's (ISRO's) newest Ku-band scatterometer which was launched on 26 September 2016 from ISRO's space-port Sriharikota on-board the PSLV C35 mission. It is an advanced follow-on of OSCAT, ISRO's first Scatterometer in space on-board the Oceansat-2 satellite, which ceased to operate in April 2014. OSCAT had been a globally acclaimed sensor during its lifetime. The data from SCATSAT-1 exhibit superior quality, and will not only serve the operational wind and weather prediction community in the years to come, but also hold the promise of securing a place in the long-term climate data records. SCATSAT-1 is a standalone scatterometer mission atop the Indian Mini Satellite (IMS-2) bus. The scatterometer payload is a two-beam, dual-polarized, conically scanning, pencil beam, real-aperture radar which measures near-surface wind vectors over ocean exploiting Bragg scattering resonance at Ku-band. It has been developed in ISRO's Space Applications Centre, Ahmedabad in less than two and half years to replace OSCAT. Although it inherits the instrument specifications from OSCAT, several enhancements have been made in its hardware as well as in the payload characterization from the purview of miniaturization and performance improvement over OSCAT. This article highlights the hardware improvements, the payload characterization methods devised, and the performance enhancements of SCATSAT-1 over OSCAT. The in-orbit performance of SCATSAT-1 is also discussed.

Keywords: OSCAT, SCATSAT-1, scatterometer, Sigma-0.

Introduction

THE worldwide demand of near real-time Ku-band scatterometer data after the premature termination of OSCAT's services necessitated a quick replacement. Hence, SCATSAT-1 has been developed and put in orbit nearly within two and a half years after OSCAT. In a way, it is similar to how Quikscat had been a quick replacement for NSCAT in 1999. This development timeline turned out to be all the more challenging because SCATSAT-1 is not a replica of OSCAT. One of the reasons behind this is that the spacecraft is different – a consequence of a mission that was hatched as an interim arrangement and so required to be standalone. The standard Indian Mini Satellite (IMS-2) bus was considered suitable for SCATSAT-1 from the resource vis-à-vis utilization perspective, and also due to the fact that this bus can be realized in a short span of time. IMS-2 is a smaller bus than the one which carried Oceansat-2. The payload configuration of SCATSAT-1 was commensurately a miniaturized version of OSCAT.

However, more than miniaturization, the instrument makeover is aimed at addressing the observations in OSCAT and for improving the system performance. This ranged from lowering the system noise floor to reducing the insertion loss of and energy leakage at the rotary joint, from improving the heat dissipation and torque capability of the scan mechanism to introducing cross-patch architecture for critical elements.

Another highlight of SCATSAT-1 is the plethora of configurable features embedded in its on-board processor, some of which are reserved for handling exigencies and the rest for improving the performance. The processor has several new elements like the two-stage digital filter replacing the analog filter in the receiver, fine-resolution 4 K Fast Fourier Transform (FFT) and 32-bit precision of on-board processed data.

The payload characterization, notwithstanding all of the above, is the forte of SCATSAT-1. The linearity of the system response that was established on ground was exactly replicated by in-orbit measurements. This and other characterizations such as brightness–temperature calibration of radiometric noise, active target simulation, calibration (Cal) power to transmit power mapping, etc. have been carried out with precise detail, the impact of which is being observed in the quality of data being served by SCATSAT-1 since its launch.

System overview

This section highlights the overall mission objectives, observation geometry and provides an overview of the sensor.

*For correspondence. (e-mail: prantik@sac.isro.gov.in)

Mission specifications

SCATSAT-1 inherits the mission specifications of its predecessor, except for a revised commitment of 25 × 25 km wind vector cell (WVC) size. This is derived from experience of generating qualified wind products over 25 sq. km WVCs from OSCAT data. The wind-speed regime is also enhanced from 2 to 24 m/s in OSCAT to 3 to 30 m/s in SCATSAT-1 based upon OSCAT experience. Table 1 enlists the major mission specifications of SCATSAT-1; the modifications with respect to OSCAT are highlighted (in bold).

Viewing geometry

Figure 1 schematically depicts the scanning pencil-beam geometry of SCATSAT-1. The salient features illustrated in Figure 1 are:

(1) The spacecraft body axes and the orbital axes are 180° out of phase in roll and pitch. This means that, unlike the usual convention, the velocity direction is aligned with the negative spacecraft body roll and the orbital positive pitch is aligned with the body negative pitch.

(2) The antenna-pointing towards spacecraft body positive pitch axis, the scan angle encoder zero-crossing and the first footprint in a scan are coincident.

(3) The antenna rotates clockwise when viewed from the spacecraft towards Earth (or equivalently counter-clockwise when viewed from the positive yaw axis). Therefore, the aft-scan follows the fore-scan during one revolution of the scanner.

(4) The Doppler centroid of the echo will traverse from zero value at 0° (first footprint location) to a maximum positive value at 90°, return back to zero at 180° and then traverse the positive maximum at 270°, before again returning to zero at 360° at the end of the scan.

(5) The scatterometer emanates two beams at two linear polarizations (*H* and *V*) and at look angles of 42.62° and 49.38° respectively. The corresponding instantaneous field of view (IFOV) dimensions are 26 km × 46 km for *H*-polarized inner beam and 31 km × 65 km for *V*-polarized outer beam.

(6) Both inner and outer beams are available in the inner qualified swath (1400 km), beyond which only the outer beam is available up to 1800 km. The spatial resolution of the scatterometer is beam width-limited azimuthally, while in the range direction it is improved by linear frequency-modulated signal (chirp) compression and frequency binning.

Figure 2 shows a schematic representation of SCATSAT-1 atop the IMS-2 bus. Figure 3 shows a few real snapshots of the hardware capturing views of the different subsystems.

Table 1. Mission specifications of SCATSAT-1

Parameters	Value
Spacecraft altitude	720 km (nominal)
Inclination	98°
Orbit	Polar, sun synchronous
Frequency	13.515625 GHz
Polarization	*HH* for inner and *VV* for outer beams
Swath	1400 km (both *HH* and *VV* beams available) 1400–1800 km (only *VV* beam available)
Wind speed range	**3–30 m/s**
Wind direction range	0°–360°
Wind speed accuracy	**1.8 m/s** rms or 10%, whichever is higher
Wind direction accuracy	20° ms
Wind vector cell (grid) size	**25 km × 25 km**

Enhancements over OSCAT

The enhancements in SCATSAT-1 over OSCAT are discussed in this section. These can be broadly categorized into enhancements in the sensor hardware elements and those in the on-board processor features.

System improvements

Digital subsystem (DSS): Three digital subsystems (digital chirp generator, payload controller (PLC), and data acquisition and compression subsystem) of OSCAT along with their redundant counterparts and corresponding electric power conditioners (EPCs) have been integrated into a single digital subsystem (using a more resourceful Virtex 4 FPGA) with its main and redundant trays and a common EPC stacked together in a single package. This has resulted in 15 kg mass reduction and 25 W power-saving.

Low-noise amplifier: A new microwave monolithic Integrated circuit (MMIC)-based low-noise amplifier (LNA) with input waveguide interface (replacing the coaxial interface in OSCAT) and improved noise figure (2.2 dB compared to 2.8 dB in OSCAT) has been realized. It is expected to achieve 1 dB improvement in overall noise figure.

Anti-aliasing filter – analog versus digital: Scan position-dependent biases were observed in OSCAT data and could be attributed, to a fair extent, to the slope of pass-band profile of the surface acoustic wave (SAW) band-pass filter at the output of the receiver. Analyses revealed that since the echo occupied different portions of the receiver spectrum (±500 kHz with respect to the centre frequency) owing to Doppler shift in the span of a scan, both signal and noise power measurements were differentially weighed by the filter profile at different scan positions. Simulations were carried out to analyse the impact of slope and ripple of the receiver filter profile on the

noise and signal-plus-noise measurements, and specifications were derived for the SAW filter. Realization of such a SAW filter with simultaneous flat passband and sharp cut-off specifications was found unrealistic. Hence, a near-flat passband and gradual roll-off discrete-device anti-aliasing filter was kept in the receiver. The DSS would, hence, sample the receiver output at 65 MHz, perform *I*–*Q* demodulation and subsequently subject the *I* and *Q* samples to two-stage filtering and decimation. This has been done because digital filters with stringent flat-band ripple and stopband rejection are easier to realize, are more stable and have no drift in performance with time compared to analog filters. Two-stage filtering was done to keep the order of the digital filter at each stage realizable through Field Programmable Gate Array (FPGA) resources.

The receiver output spectrum centred at ±15.625 MHz was down-converted to baseband (by virtue of quadrature demodulation), filtered (1st stage) and decimated by a factor of 16, and then again filtered and decimated by a factor of 2 with the final sampling frequency of 1.953 MHz and a passband of 1550 kHz.

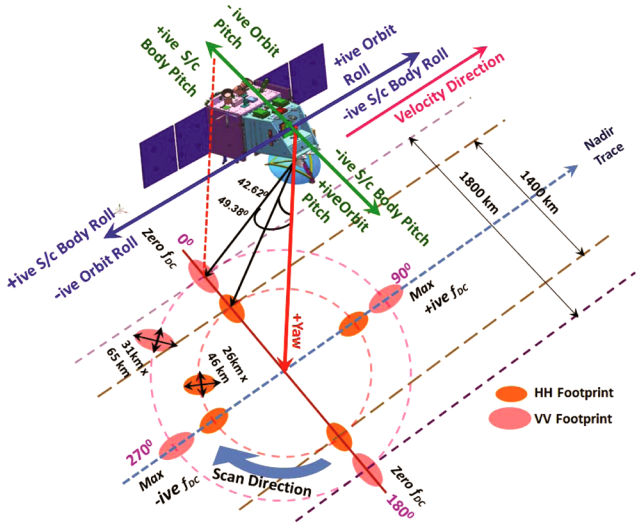

Figure 1. Viewing geometry of SCATSAT-1.

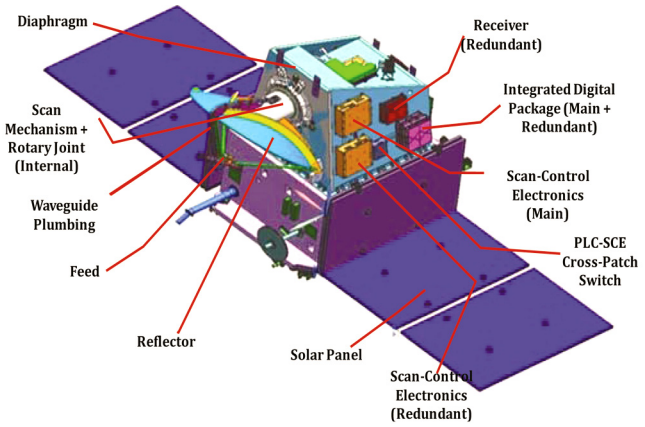

Figure 2. SCATSAT-1 atop IMS-2 bus (schematic view).

Rotary joint: An improved version has been designed and manufactured in-house with fewer joints, better insertion loss (0.3 and 0.2 dB for *H*- and *V*-channels), stable performance with rotation, high inter-channel isolation (~50 dB), and better electromagnetic interference and susceptibility performance without epoxy treatment.

Scan mechanism: A new Halbach motor has been used which can generate more torque with less current consumption. Also, the material of the shaft has been changed from titanium to stainless steel for better heat dissipation. Redundancy has been introduced in the scan-start reference signal generation by adding an external Hall sensor (which symbolizes zero-crossing angle reference, and can be synchronized with payload operations and angle data), so that payload operation is not limited by the fallibility of the scan-angle encoder.

Cross-patch architecture: OSCAT ceased to operate because of failure of one subsystem in the main chain and one in the redundant chain. The scan angle encoder in the main chain malfunctioned and when switched over to the redundant chain, the travelling wave tube amplifier (TWTA), which was in cold storage in orbit for four and half years, failed to boot. Since the main and redundant chains were mutually exclusive end- to-end, two disconnected failures led to shut down of the payload. Hence, cross-patch architecture has been introduced between main and redundant packages of critical subsystems in SCATSAT-1. These include a cross-patch between PLC and scan control electronics (SCE), and another between the frequency generator (FG) and the TWTA.

On-board processor enhancements

The enhancements in the on-board processor are illustrated here.

Doppler compensation: While de-chirping the received energy, the on-board processor uses a Doppler-shifted replica of the transmitted chirp to compensate rotation-induced Doppler in the echo. The Doppler shift due to rotational scan (f_{DC}) is computed on-board at every pulse repetition interval (PRI). All parameters of this equation can be modified through ground command.

$$f_{DC} = \frac{[-]2[v_s]\sin[\theta_{look}]\sin([\phi_{az}]+[\Delta\phi_{az}])}{\lambda}, \quad (1)$$

where v_s is the real-time spacecraft velocity data, θ_{look} the preloaded value of pointing angle, but modifiable through command uplink and ϕ_{az} is the real-time angle encoder

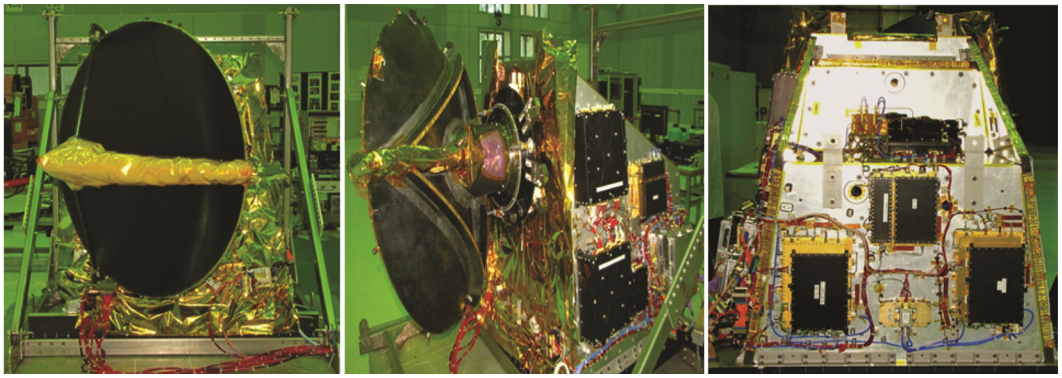

Figure 3. Snapshots capturing different views of SCATSAT-1 scatterometer.

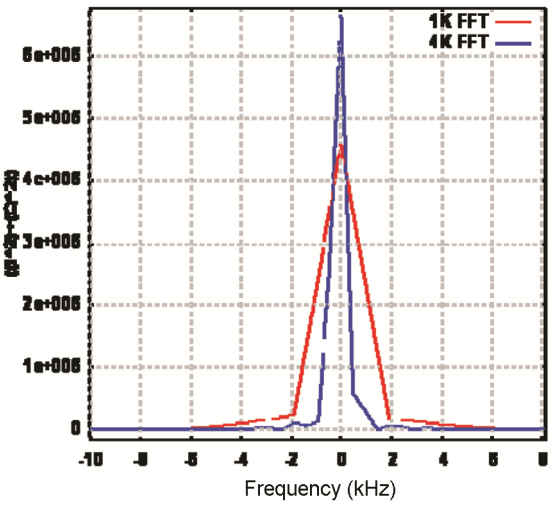

Figure 4. Comparison of spectral response between overlapped 1 K FFT and 4 K FFT.

reading obtained from SCE. The up-linkable $\Delta\phi$ feature has been included in SCATSAT-1 in order to negotiate any angular offset between the angle-encoder reading and the beam pointing in the azimuth plane about the yaw axis.

Fast Fourier Transform processor: The FFT processor in Oceansat-II scatterometer followed the overlapped periodogram estimation approach. The Oceansat-II adoption of Welch's method was, however, oriented towards on-board processor memory limitations. Instead of computing 4 K FFT, the deramped signal was partitioned into seven blocks of 1 K samples, each with 50% overlap, 16-bit complex 1 K FFT operation was carried out on each block in sequence, and finally the seven 1 K FFT blocks were added element-by-element. SCATSAT-1 employs single-shot 4 K-FFT operation. This will improve FFT resolution by a factor of 4, resulting in sub-slice width reduction from 1.9073 kHz to 476 Hz. This in turn will improve spectral resolution of the estimated data. Figure 4 shows a comparison of the spectral resolution as a result of 1 K and 4 K FFT operations.

Processed data bit-precision: OSCAT data provided excellent support to studies on freeze and thaw cycles of polar ice caps. However, there were several events of data saturation over snow. This was because the 32-bit processed data were truncated by the on-board processor to 16 bits and dispatched to ground. Hence, SCATSAT-1 captures the full 32-bit precision of processed data. SCATSAT-1 data have not shown any saturation over polar ice caps and also exhibit greater dynamic range of σ^0 than OSCAT.

Bandwidth compartments, noise measurement scheme and slice-binning: OSCAT had a unique scheme of partitioning the deramped spectrum into signal-plus-noise and noise-only compartments[1]. The deramped echo spectrum will have uncompensated frequency components emanating from range drifts owing to topographic and/or latitudinal variations and pointing inaccuracies as well as from Doppler shifts due to the earth's rotation. In order to make room for such frequency drifts, the central 305 kHz segment of the receiver bandwidth is allocated for measurement of the return signal. The signal-plus-noise bandwidth is frequency binned by the on-board processor to generate range gates or slices of selectable resolution. The remaining portion of the receiver bandwidth is comprised of two spectral compartments of 622.5 kHz each, which are occupied only by noise. The noise power in each of these sidebands is integrated on-board to generate a couple of noise samples (N1 and N2) at every PRI, which are used on ground to estimate noise power in a range slice.

$$\hat{P}_{\mathrm{N,slice}} = \frac{P_{\mathrm{N1}} + P_{\mathrm{N2}}}{\mathrm{Bw}_{\mathrm{noise}}} \mathrm{Bw}_{\mathrm{slice}}, \tag{2}$$

where $\hat{P}_{\mathrm{N,slice}}$ is the estimated noise power of a slice, P_{N1} and P_{N2} are the values of N1 and N2, $\mathrm{Bw}_{\mathrm{noise}}$ the noise bandwidth and $\mathrm{Bw}_{\mathrm{slice}}$ is the slice bandwidth. The signal power in a range-slice is subsequently estimated by subtracting the noise estimate from the measured signal-plus-noise power

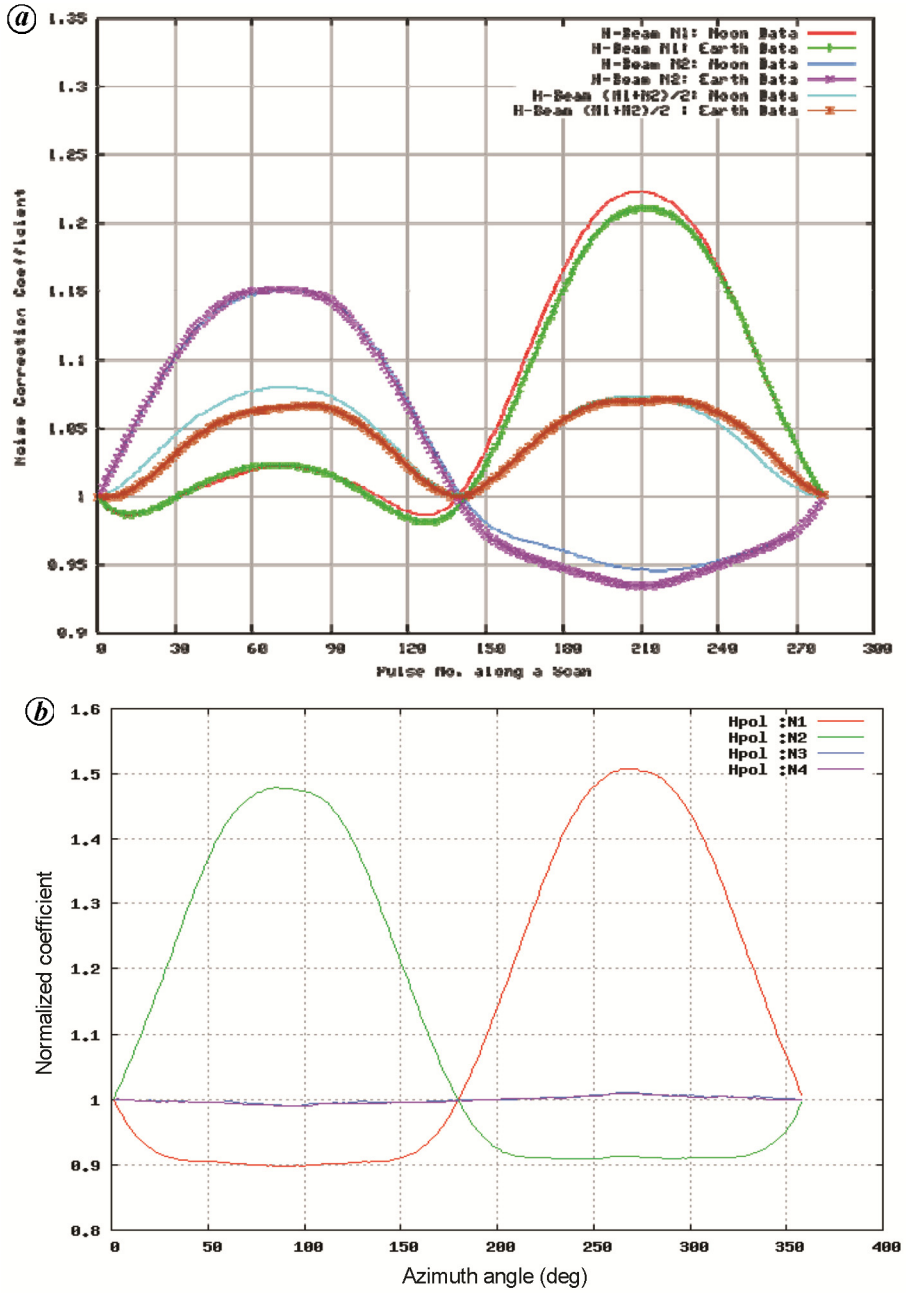

Figure 5. Scan position-dependent variation of noise measurements in (***a***) OSCAT and (***b***) SCATSAT-1; variation of the alternate noise measurement to be noted.

$$\hat{P}_{\mathrm{S,Slice}} = P_{S+N} - \hat{P}_{\mathrm{N,Slice}}, \tag{3}$$

where $\hat{P}_{\mathrm{S,slice}}$ is the signal power estimated over the slice bandwidth and P_{S+N} is the measured value. In SCATSAT-1, provision has been made for selecting the position and width of both signal and noise compartments through command uplink. This is an additional immunization measure against such problems as encountered initially in Oceansat-II (ref. 1) wherein due to mismatch between antenna pointing and angle reading, the echo was being erroneously compensated leading to signal intruding upon the noise compartments.

The two noise-only sidebands, N1 and N2, on either side of the signal-plus-noise band exhibited scan position-dependent biases in OSCAT. The reason for this variation is convolution of the entire spectrum with Doppler-shifted chirp replica in the deramping process and subsequent compartmentalization of the noise-only sidebands. In addition, there was further modulation owing to a slope in passband profile of the receiver. Analyses revealed that, since the echo occupied different portions of the receiver spectrum (± 500 kHz with respect to the centre frequency) owing to Doppler shift in the span of a scan, both signal and noise power measurements were

differentially weighed by the filter profile at different scan positions. The pattern in Figure 5 *a* was not visible on convolving the receiver noise with Doppler-shifted chirp, but could be reproduced by incorporating the receiver frequency profile into the simulation (see eqs (4) and (5)).

$$N(f) = F[\ddot{n}(t)h(t)\exp(j\pi\mu t^2)\exp(-2j\pi f_{DC}t)]. \quad (4)$$

where $N(f)$ is the convolved noise spectrum and $\ddot{n}(t)$ is the profile-weighed noise sample obtained as

$$\ddot{n}(t) = F^{-1}[W_{Rx}(f)F[n(t)]], \quad (5)$$

where $W_{Rx}(f)$ is the receiver frequency profile, $n(t)$ the Gaussian noise sample and F^{-1} is the inverse Fourier transform operator. The signal-plus-noise and noise-only compartments of $N(f)$ were found to retain the scan-dependence signatures (Figure 5 *a*) identical to the data-derived patterns.

Hence, it was decided to have a noise measurement scheme in SCATSAT-1 which will not be corrupted by the on-board signal processor. This requirement gave rise to the concept of two additional noise measurements (viz. N3 and N4), in which both f_{DC} compensation and deramping would be bypassed. Any one of them can be used in either fore- or aft-scan depending upon which segment of the bandwidth the echo is traversing for the corresponding portion of the scan. The resultant effective noise measurement, designated N5 (either N3 or N4) is fairly constant over the entire scan (Figure 5 *b*).

Pre-launch characterization and in-orbit performance

Radiometric calibration

Detection and discrimination of rain-induced roughness on the ocean surface and the resultant back scatter increase are an essential feature of wind-retrieval from the scatterometer. In the absence of an accompanying radiometer equipped with rain observation channels, the scene noise measurements from the Ku-band scatterometer are the only source of co-temporal and coincident information on rain occurrence. These noise measurements are, however, not calibrated in real time as is done in the case of conventional spaceborne radiometers. OSCAT, for example, was never calibrated for brightness temperature (T_B). Moreover, such noise measurements have the inherent limitations of low bandwidth and small integration time, and hence, have poor sensitivity.

Pre-launch two-point radiometric calibration of the instrument was carried out in the clean room using a microwave absorber soaked in liquid nitrogen bath as the cold reference and a similar absorber at laboratory ambient temperature serving as the hot reference in order to derive T_B conversion coefficients for SCATSAT-1. The T_B coefficients, thus derived through on-ground calibration, were refined on the first day of SCATSAT-1 operations using deep-space noise readings as the cold reference and pre-launch laboratory calibration for the hot reference. The spacecraft was roll-steered to make the scatterometer antenna point towards deep space, which serves as an extremely stable cold target. The scatterometer-derived T_B was found to have the similar dynamic range as collocated Advanced Microwave Scanning Radiometer-2 (AMSR-2) 10 GHz channel brightness, while the noise equivalent sensitivity over 1.6 MHz instantaneous noise bandwidth and 2 ms data window was 11 K. SCATSAT-1 periodically observes at the deep space (once in six months) and the T_B calibration is updated, if necessary.

Active target simulator

Oceansat-II suffered an initial setback in orbit when it was discovered that its antenna pointing and the corresponding angle-encoder reading were mutually offset by 210°. The on-board Doppler compensation software could accommodate 180° misalignment by virtue of a provision kept for ground-commanded sign reversal. The remnant 30° could not be entirely compensated. The spacecraft was yaw-steered by 20° as a compromise between the operational requirements of OSCAT and its sister payload, the Ocean Color Monitor. OSCAT lived its life with a residual 10° offset.

In order to ensure mutual alignment of pitch axis-pointing of the antenna and scan angle encoder zero-crossing, independent of the mechanical axes alignment, a new experiment with active target simulator has been devised. In this experiment, the target is simulated as an active source using a Ku-band horn antenna. The horn is fed with a chirp riding upon a fixed offset from the scatterometer operating frequency. The horn is fixed on a tripod and positioned in the line-of-sight with a particular orientation of the scatterometer antenna. The scatterometer is configured in receive-only mode and the antenna is rotated slowly. As already known, the received signal in every echo window is being compensated by the Doppler centroid that is computed by the PLC using angle information from the SCE. Therefore, the position of the f_{DC} compensated and deramped peak should be near-zero when the scatterometer antenna is directed towards the horn. The hypothesis and observations were found to be in absolute agreement.

The active horn set-up was utilized for verification of adjustable f_{DC} computation as well as demonstration of the flexible bandwidth positioning feature of the signal processor on-board SCATSAT-1. The transmitted signal from the horn was a chirp with a Doppler shift which was offset (both ahead and behind) from that pertaining to the

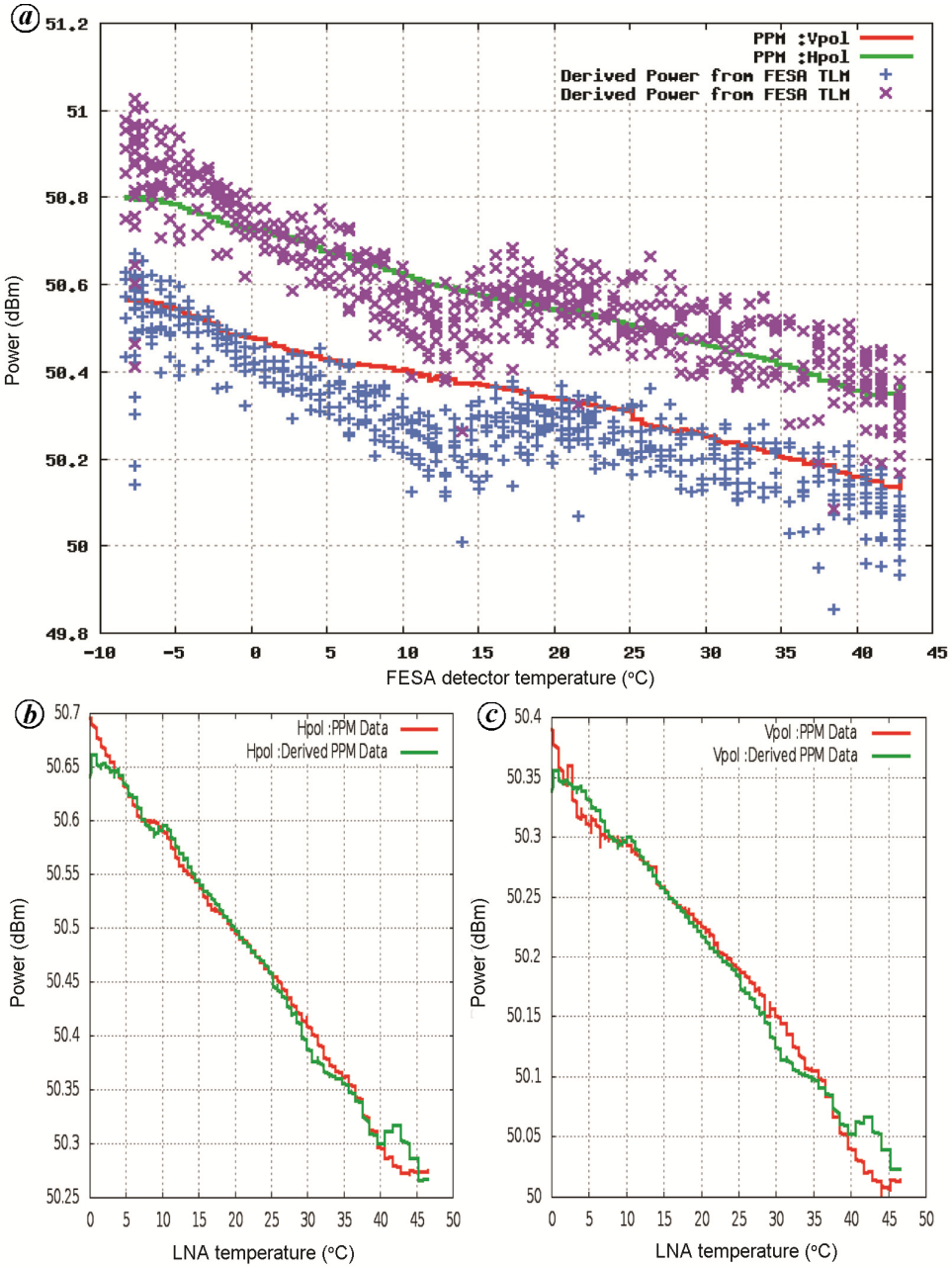

Figure 6. Characterization of TWTA output power measured over peak power meter versus Front-end Switch Assembly (FESA) telemetry across temperature excursion (***a***), versus mapped calibration-power for *H*-polarization (***b***) and for *V*-polarization (***c***).

azimuth angle of the scatterometer antenna beam. The resultant Doppler compensation by the on-board processor drove the deramped signal to positive and negative extremes in the two cases. The S + N band was shifted accordingly in the two cases and the deramped spectrum was captured in the central bins in both the cases for both the beams.

Calibration power characterization

During transmission, the pulsed power from the TWTA is asynchronously monitored by a diode detector positioned prior to the FESA output beam selection switch. The etected power is telemetered to the PLC. The transmit power is also coupled to the receiver port through a 100 dB isolator. This serves as an internal calibration loop. The OSCAT calibration-power for both beams exhibited a repetitive pattern of variation over an orbit with peak-to-peak excursion of ±0.5 dB. The cause of this variation could not be definitely identified and, in spite of several hypotheses and post-facto adjustments, the calibration power estimate error remained a cause of remnant biases in OSCAT data.

In case of SCATSAT-1, the two sources of transmit power monitoring have been characterized against the

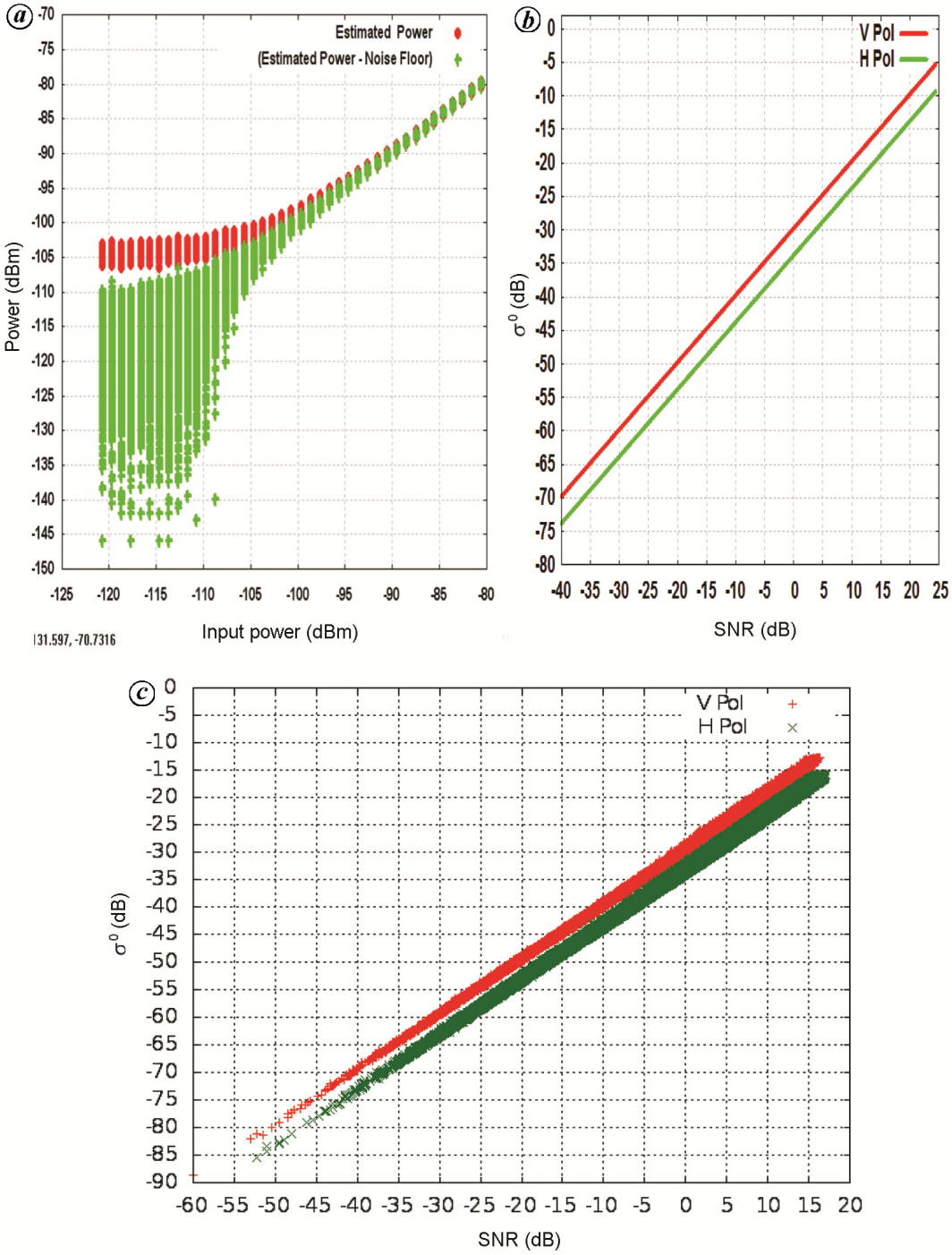

Figure 7. ***a***, Power transfer curve (input power versus input power estimated from output power) with and without noise-floor correction. ***b***, Signal-to-Noise Ratio (SNR) versus σ^0 derived from pre-launch ground characterization. ***c***, SNR versus σ^0 derived from in-orbit observation.

actual transmit power measured on a peak power meter (PPM) across a temperature excursion in vacuum. Figure 6 shows the results. It can be seen that characterization of the FESA diode detection, which is asynchronous with the pulse duration and not available in every PRI, is accurate within ±0.1 dB about the PPM readout (Figure 6 *a*). The calibration power almost exactly matches with the PPM readout for both H-pol (Figure 6 *b*) and V-pol (Figure 6 *c*) over the entire temperature range. The FESA telemetry was envisaged as an alternate source of transmit power information. However, calibration power in case of SCATSAT-1 has been found to be extremely stable in orbit. Thus, another vital source of bias from OSCAT experience has been successfully addressed in SCATSAT-1.

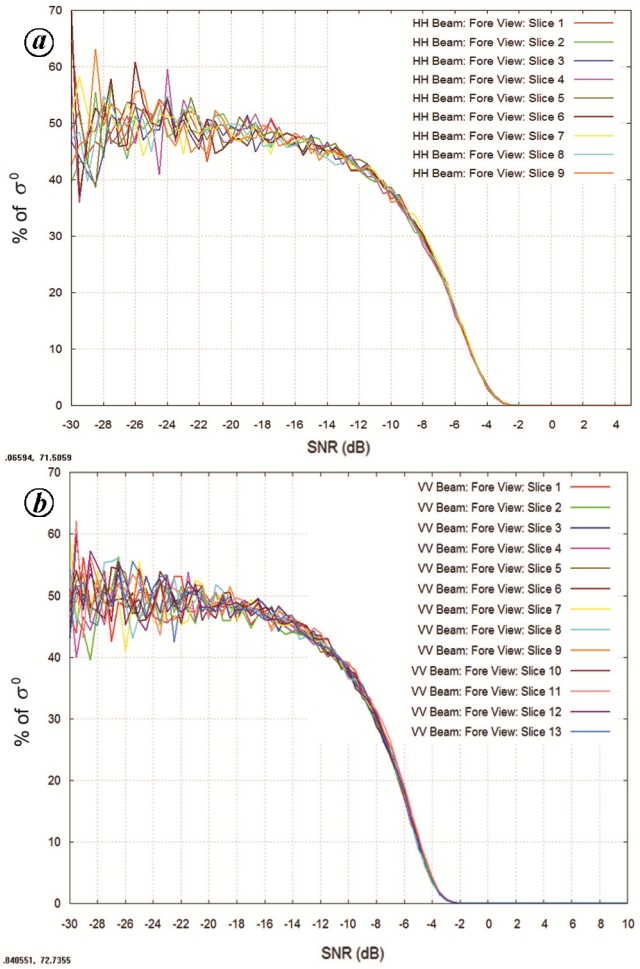

Figure 8. ***a***, SNR versus percentage of negative σ^0 – *HH*-beam. ***b***, SNR versus percentage of negative σ^0 – *VV*-beam.

Rx path characterization

One of the distinctive features of SCATSAT-1, which gives it an edge over OSCAT, is its receive-path characterization. The power transfer curve from the rotary joint to the receiver output was mapped in steps of 1 dB over the entire dynamic range and even up to 10 dB below the noise floor. The nonlinearity of system response at and around the noise floor was precisely captured (Figure 7 *a*). Hence, the system noise floor, which was calculated from noise figure measurements using Y-factor method, was subtracted from the power transfer curve. Thus the scatterometer principle of noise subtraction was utilized in characterizing the scatterometer itself and in establishing the linearity of the system response. This was converted to the linearity between SNR and σ^0 as shown in Figure 7 *b*. The linearity between SNR and σ^0 estimated from the data in-orbit exactly matches with the ground characterization (Figure 7 *c*) as do the noise-equivalent σ^0 values (–33 dB for *HH* and –30 dB for *VV* beam).

Noise estimation quality

The percentage of negative σ^0 as a function of SNR is a vital statistical tool for characterizing the noise estimation and correction accuracy of scatterometer[1]. The fact that negative σ^0 statistically saturates at 50% at poor-SNR conditions (<–10 dB) makes it a useful tool for noise-calibration. A remnant bias in noise should show up as an anomalous percentage of negative σ^0 if similar statistics were extracted from the actual data.

The percentage of negative σ^0 was calculated for SCATSAT-1 over cumulative data of one revisit cycle i.e. two days. It can be seen that the percentage of negative σ^0 saturates at 50% for –30 dB SNR across all range-slices for *HH*-beam (Figure 8 *a*) and *VV*-beam (Figure 8 *b*). This is all also indicative of the fact that all the range-slices of both beams are balanced as their SNR versus negative σ^0 curves are matched within 0.5 dB dispersion.

Conclusion

This article introduces the SCATSAT-1 instrument to the community. It sums up the system enhancements in SCATSAT-1 over its predecessor OSCAT and also much of the payload characterization methods adopted and their impact being seen in the data quality post launch.

1. Misra, T. *et al*., Oceansat-II scatterometer: sensor performance evaluation, σ^0 analyses and estimation of biases. *IEEE Trans. Geosci. Remote Sensing*, 2014, **52**(6), 3310–3315.

doi: 10.18520/cs/v117/i6/941-949